Supplementary Information for 'Stacking structure in liquid polyaromatic hydrocarbons'

Thomas F. Headen,*,† Neal T. Skipper,‡ and Michael P. Hoepfner¶

†*ISIS Neutron and Muon Source, Rutherford Appleton Laboratory, Harwell Campus, Oxon, OX11 0QX*

‡*Dept Physics and Astronomy, University College London, Gower Street, London, UK, WC1E 6BT*

¶*University of Utah, Department of Chemical Engineering, 50 South Central Campus Drive, Salt Lake City, Utah 84112, United States.*

E-mail: tom.headen@stfc.ac.uk

S1 Experimental and Data Refinement Methods

In a neutron total scattering experiment, the measured quantity is the differential scattering cross-section. With appropriate corrections, this measurement provides the total structure factor, $F(Q)$. Neutrons interact with nuclei, so the scattering length, b_i, varies between different isotopes of the same element. In particular, hydrogen (with $b_H = -3.74$) can be conveniently replaced by deuterium (with $b_D = 6.67$). By conducting experiments on many samples with different isotopic substitutions, we can obtain more precise radial and orientational correlations, as the complementary data from these samples provide strong constraints on structure refinement techniques.

Typically, we measure multiple data sets, $F_i(Q)$, each representing the same chemical composition but with a unique isotopic composition. The corrected diffraction data is then

a weighted sum of the different partial structure factors arising from distinct atom pairs α,β.

$$F_i(Q) = \sum_{\alpha,\beta \leq \alpha} (2 - \delta_{\alpha\beta}) c_\alpha c_\beta b_\alpha b_\beta \left(S_{\alpha\beta}(Q) - 1 \right), \tag{S1}$$

where c_α is the atomic fraction of species α, b_α is the neutron scattering length of atom α, $Q = 4\pi(\sin\theta)/\lambda$ is the magnitude of the momentum change vector of the scattered neutrons of wavelength λ, Kroneker delta $\delta_{\alpha\beta} = 1$ when $\alpha = \beta$ and zero otherwise and $S_{\alpha\beta}(Q)$ are the Faber-Ziman partial structure factors.

The Faber-Ziman structure factors can be related to the real-space structure, in terms of partial radial distributions functions $g_{\alpha\beta}(r)$, by a Fourier Transform:

$$S_{\alpha\beta}(Q) - 1 = \frac{4\pi\rho_0}{Q} \int_0^\infty r \left(g_{\alpha\beta}(r) - 1 \right) \sin(Qr) \mathrm{d}r, \tag{S2}$$

where ρ_0 is the atomic number density of the sample.

One can also take a inverse Fourier Transform of the measured $F(Q)$ to yield the pair distribution function, or total radial distribution function $f(r)$:

$$f(r) = \frac{1}{(2\pi^3\rho_0)} \int_0^\infty 4\pi Q^2 F(Q) \frac{\sin Qr}{Qr} \mathrm{d}Q, \tag{S3}$$

which, in analogy to the total structure factor is the weighted sum of all the partial pair distribution functions in the system:

$$f(r) = \sum_{\alpha,\beta \leq \alpha} (2 - \delta_{\alpha\beta}) c_\alpha c_\beta b_\alpha b_\beta \left(g_{\alpha\beta}(r) - 1 \right), \tag{S4}$$

Neutron total scattering data were measured at the Near and Intermediate Range Order Diffractometer (NIMROD) and the ISIS Neutron and Muon Source, Rutherford Appleton Laboratory, UK. NIMROD in as time-of-flight neutron diffractometer on the second target station viewing both the cyrogenically cooled hydrogen moderator, and the thermal water pre-moderator. This, coupled with a large array of forward scattering scintillator detectors

from $2\theta = 0.5 - 40°$, give an exceptionally wide Q-range ($Q = 0.02 - 50\text{Å}^{-1}$). In addition the use of high energy neutrons (thermal and epithermal), detected at low scattering angles, reduced inelastic scattering effects that can be difficult to correct for in samples containing light hydrogen. It is therefore an ideal instrument with which to study liquid samples using H/D substitution.[1]

For both pyrene and phenathrene systems neutron scattering data were collected for fully hydrogenated (pyrene: Sigma puriss p.a. $\geq$ 99%, phenanthrene: Aldirch, sublimed grade $\geq$ 99.5%), fully deuterated (pyrene-d10: CDN isotopes, 99.5%-d10, phenanthrene-d10: CDN isotopes 98.5%-d10), and a 1:1 molar ratio of the hydrogenated and deuterated samples. The samples were loaded into null coherent scattering TiZr cells of 1mm path length by loading in powder, melting the sample in a vacuum oven (TiZr should not be heated in air at the melting temperatures) and then, were appropriate, toping up with more powder. The loaded sample cells were then placed on an oil-bath heated "hot-stick" positioned such that the incident beam only viewed the bottom section of the cell. The incident beam was defined using six sets of jaws such that the beam on the sample had dimensions 30mm $\times$ 15mm ($H \times$ V). Samples were heated to a few degrees above their melting points (391K for phenanthrene and 433K for pyrene). Melting was observed by loss of Porod scattering at low Q and loss of Bragg peaks at high Q. Minimum counting times were 2 hours for deuterated samples, and 3 hours for hydrogenated samples. To allow for data correction and calibration, scattering data were also collected from the empty instrument, the empty sample cell, and a null coherent scattering Vanadium-Niobium alloy standard slab of thickness 3 mm. Background subtraction, and multiple scattering, absorption, and normalization correction procedures were performed using GUDRUN,[2] to give the interference differential scattering cross-section for each isotopically distinct sample. Particular attention needs to be paid to correction of inelasticity effects, especially for the samples containing hydrogen. The self-scattering background and inelasticity effects were removed from the total differential scattering cross section using an iterative method developed by Soper.[3,4]

The total neutron scattering data were analysed by the simulation based refinement technique Empirical Potential Structure Refinement (EPSR). In essence the technique generates a 3-dimensional ensemble of molecules that aligns with the measured scattering data by using this data to constrain and refine a classical molecular simulation of the system. The detailed theory behind EPSR is described elsewhere.[5] Briefly, the method begins with an equilibrated Monte Carlo simulation based on initial "reference" potentials. It then iteratively adjusts an empirical potential as perturbation on top of the seed potential, calculated using the difference between the measured and simulated structure factors, until the molecular ensemble matches the scattering data. This approach enables the incorporation of prior knowledge—such as molecular geometry and density, and reasonable chemical physics of the system - such as the seed potentials and partial charges - to be included into the refinement process. It is also a maximum entropy method, producing the most disordered, and therefore most likely structure, given the above constraints and fit the data.

For both phenanthrene and pyrene, EPSR simulations where conducted using epsr26.[6] Each simulation box contained 500 molecules, with the cubic simulation box size chosen to match the density of the liquid at the measured temperature determined from interpolation of values for liquid densities as a function of temperature from the DETHERM database.[7–9] Reference potentials (LJ and partial charge) where obtained for the OPLS-AA force-field using the LigParGen facility,[10] with C-H bond lengths changed slightly to give a close match to the C-H bonding peak in the experimentally determined $f(r)$. Dihedral constraints were applied across all bonds in the molecules to maintain planarity of the aromatic ring, with disorder within the molecule adjusted using the vibrational, angular and dihedral temperatures within EPSR to match the local structure as determined by experimental $f(r)$ (phenanthrene: $T_{vib} = 35K, T_{ang} = 3, T_{dih} = 10$, pyrene: $T_{vib} = 65K, T_{ang} = 1, T_{dih} = 1$, noting that the angular temperatures are defined in the EPSR software relative to the vibrational temperature, and the dihedral temperature is a parameter which describes how close dihedrals should be to their equilibrium values, and are therefore both unit-less). After an initial

period of equilibration using the reference potentials, the additional empirical potential was added, with a maximum energy amplitude (ereq) of 10 kJ/mol.

S2 Real space $f(r)$ comparison for EPSR models

Simulated and experimental structure are compared in momentum, Q space (see figure 2 in main text), but can also be directly compared in real space. The total radial distribution function is a weighted sum of all the partial pair correlations in the system and can be obtained experimentally through a Fourier Transform of the $F(Q)$ (see equations S3 and S4). Figures S1 and S2 show the simulated and experimental $f(r)$ for phenanthrene and pyrene respectively. The quality of fit is excellent demonstrating the appropriateness of the molecular structures used in the simulation.

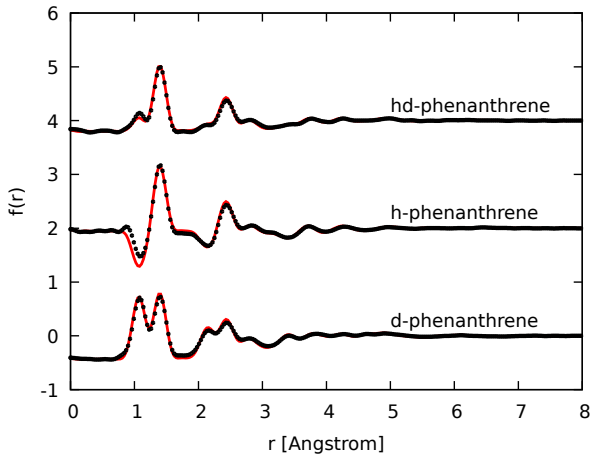

Figure S1: Measured (dots) and EPSR simulated (red line) $f(r)$ for three isotopologues of liquid phenanthrene.

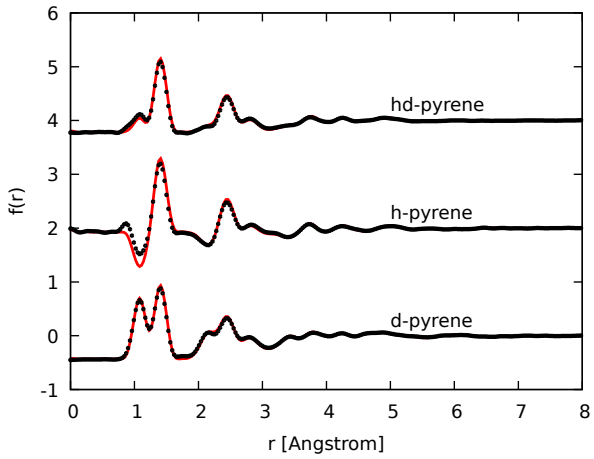

Figure S2: Measured (dots) and EPSR simulated (red line) $f(r)$ for three isotopologues of liquid pyrene.

S3 EPSR fit compared to reference potentials and standard OPLS charges

Figures S3 and S4 below show the improvement in the fit to $F(Q)$ with the addition of the EPSR refined potentials compared to simulations with the reference potentials only. There is a clear improvement in fit, particularly at lower Q values which are dominated by the intermolecular correlations.

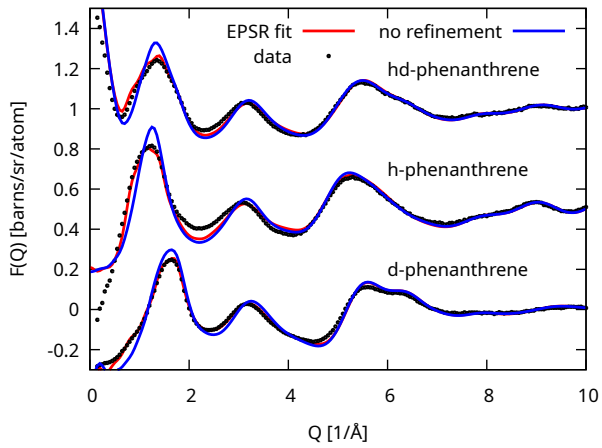

Figure S3: Experimental $F(Q)$ and simulated fits with and without refinement for liquid phenanthrene.

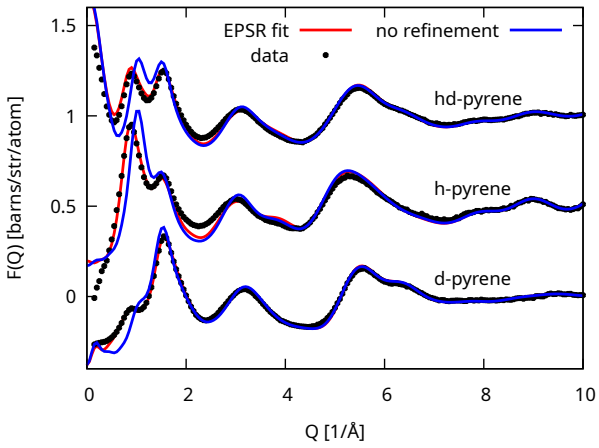

Figure S4: Experimental $F(Q)$ and simulated fits with and without refinement for liquid pyrene.

In addition to the above, we explored the consistency of refined fits and the resulting structure through running an alternative EPSR refinement with a slightly different reference potentials. In addition to the potential presented in the main text, which uses partial charges generated from a semiemperical (AM1) calculation in the LigParGen server,[10] we also have used the "standard" OPLS partial charges of -0.115 for C(H) atoms, +0.115 for H(C) atoms and 0.000 for fused carbon atoms (as used for our previous study of liquid naphthalene[11]). As shown in Figures S5 and S6 the quality of the fit is very similar.

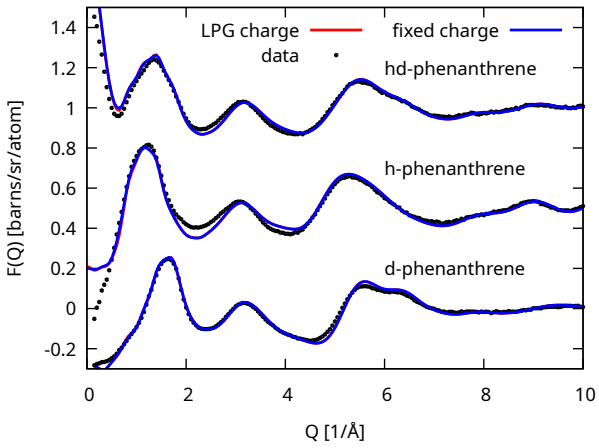

Figure S5: Experimental $F(Q)$ and simulated scattering for liquid phenanthrene from EPSR refined models with different seed potentials for partial charges. LPG is using charges generated by LigParGen server, fixed charges are the standard OPLS charges for aromatics as described above.

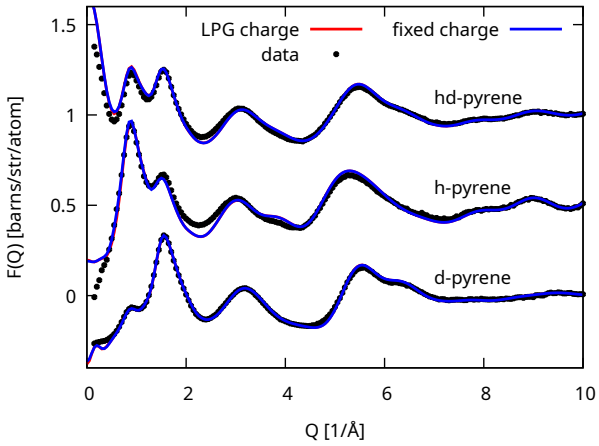

Figure S6: Experimental $F(Q)$ and simulated scattering for liquid pyrene from EPSR refined models with different seed potentials for partial charges. LPG is using charges generated by LigParGen server, fixed charges are the standard OPLS charges for aromatics as described above.

S4 Full Angular Radial Distribution Functions for Phenanthrene and Pyrene

Below in figures S7 and S8 are the full angular radial distribution functions ($g(r,\theta)$) for liquid phenanthrene and pyrene as a function of the angle between the aromatic planes, θ. This is calculated by:

$$g(r,\theta) = \frac{\Delta(r,\theta)}{\frac{2}{3}((r+\Delta r)^3 - r^3).\sin\theta.\Delta\theta.\rho} \tag{S5}$$

where $\Delta n(r,\theta)$ is the is the number of molecules in the distance range $r+\Delta r$ and angle range, $\theta+\Delta\theta$; ρ is the bulk number density and the $1/\sin\theta$ factor corrects for the θ dependence of the solid angle when integrating over the azimuthal angle.

For both phenanthrene and pyrene it is clear that parallel interactions are preferred over perpendicular nearest neighbour interactions. Interestingly of phenanthrene there is a short range shoulder at $r \approx 5$Å and $\theta = 90°$ which could be due to an interlocking arrangement of the concave sections of the molecule.

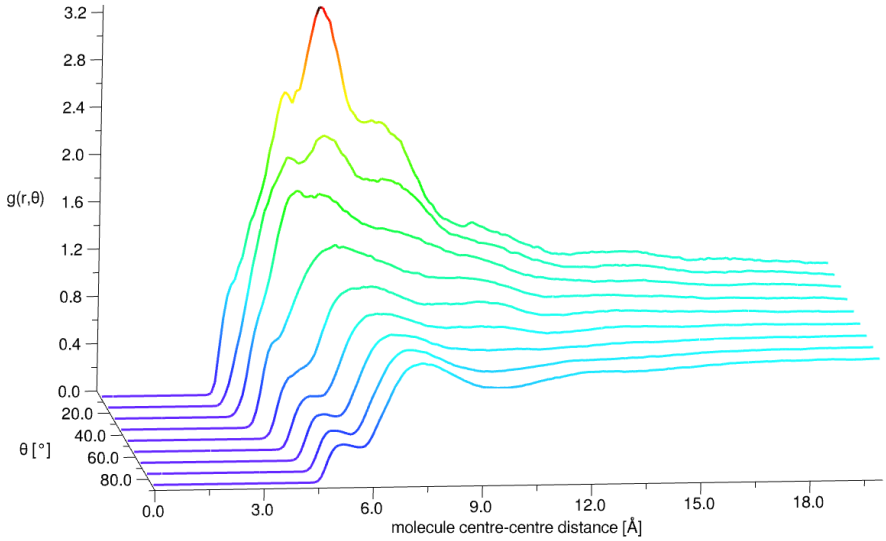

Figure S7: Angular radial distribution function, $g(r, \theta)$, for liquid phenanthrene, where θ is the angle between the aromatic planes.

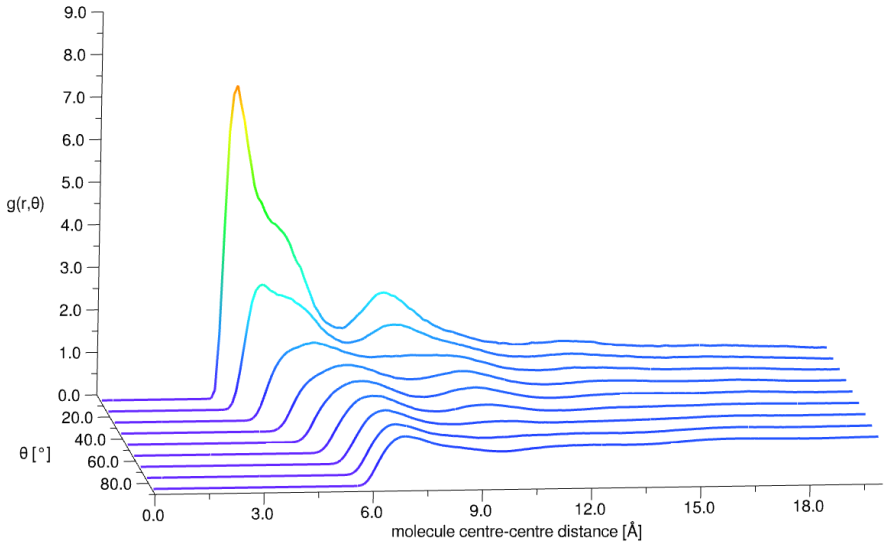

Figure S8: Angular radial distribution function, $g(r, \theta)$, for liquid pyrene, where θ is the angle between the aromatic planes.

As discussed in the main text, in addition to the reference potential provided by the

LigParGen server (with partial charges from an AM1 semi-empirical calculation), we also used standard OPLS force-field with partial charges fixed charges to follow what we used in the studies of naphthalene and benzene. As shown in figures S5 and S6 this change in reference potential does not strongly effect the quality of fit once the simulations are refined to the data. In Figures S9 and S10 below we plot the angular radial distribution functions for both refined simulations. The ARDF's of phenanthrene are very similar with perhaps a slight preference for shorter range interactions at low angle for the OPLS fixed charge case. For pyrene there is a clearer difference, with a stronger preference for parallel stacked interactions for the OPLS fixed charge seed potential. We should note here that there is a $\sin\theta$ normalisation term in the calculation of $g(r,\theta)$ which amplifies small absolute changes in coordination numbers at low θ. Nevertheless the conclusions that pyrene shows the strongest level of stacking is still very much valid, no mater which reference potential is used.

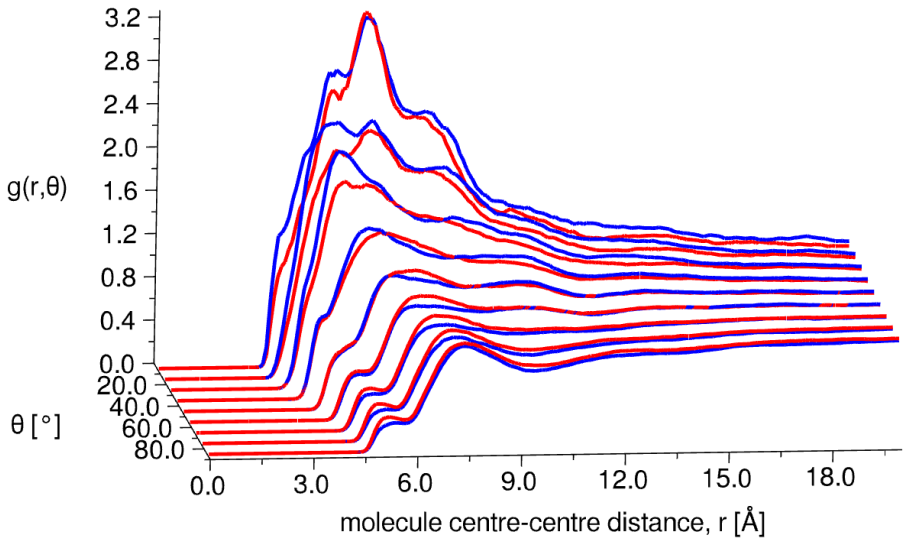

Figure S9: Angular radial distribution function, $g(r,\theta)$, for liquid phenanthrene, where θ is the angle between the aromatic planes, using different partial charge schemes: red = LiParGen, blue = OPLS fixed charges.

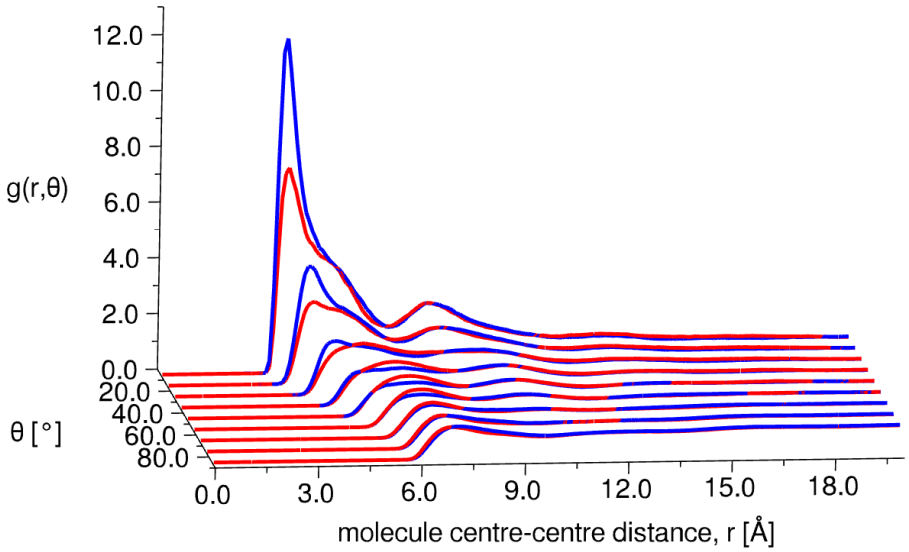

Figure S10: Angular radial distribution function, $g(r, \theta)$, for liquid pyrene, where θ is the angle between the aromatic planes, using different partial charge schemes: red = LiParGen, blue = OPLS fixed charges.

We can also use alternative axes to further understand relative orientations. In figure S11 below we plot the angular distribution function as function of the angle between the long (x) axes, ϕ for liquid pyrene. This shows that at short distance where the molecules are stacked (see figure S8) the long axes are also aligned, showing that a "cross" dimer is not observed and that, taking into account the SDF's, full face-to-face staking is preferred.

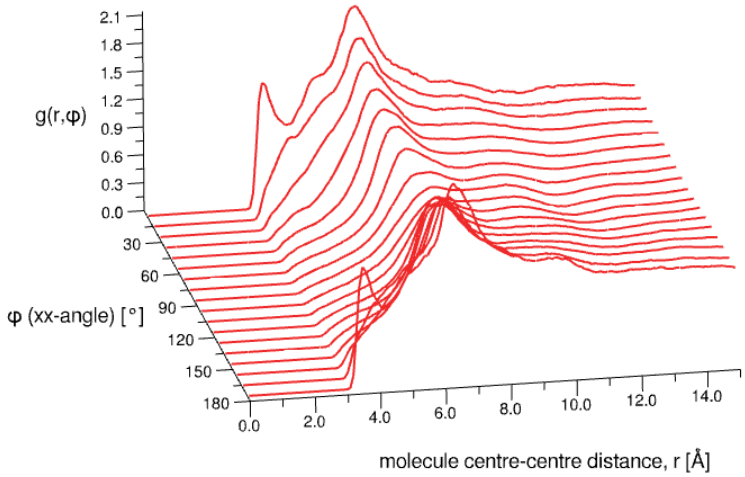

Figure S11: Angular radial distribution function, $g(r, \phi)$, for liquid pyrene, where ϕ is the angle between the long axes (x).

S5 Selected slices in spatial density functions

Figures S12 and S13 plot two dimensional slices through the three-dimensional spatial density function for phenanthrene-phenanthrene correlations. The voxel size for the SDF calculation is 0.5Å and interpolation has been used in the 2d plot for greater clarity. Throughout this work the x axis corresponds to the long axis of the molecule and the z-axis corresponds to the normal to the aromatic plane. The main correlation in the xy plane is in the "bay" of the phenanthrene molecule and likely corresponds to molecules at 90° to each other in an interlocked fashion, as seen as a shoulder in S7.

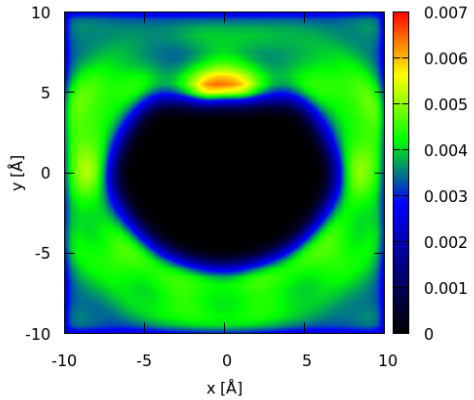

Figure S12: 2d slice through the phenanthrene-phenanthrene spatial density function in the xy plane (i.e. in the plane of the molecule).

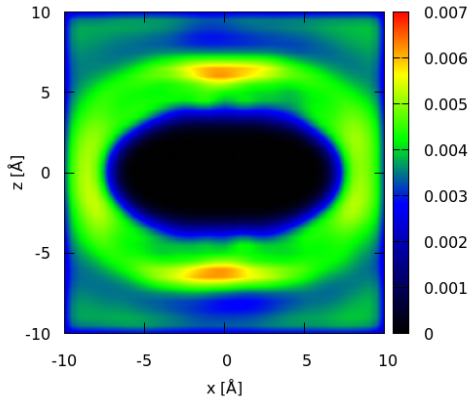

Figure S13: 2d slice through the phenanthrene-phenanthrene spatial density function in the xz plane where x is the long axis of the molcule and z is the axis normal to the aromatic plane.

Figures S14 and S15 plot two dimensional slices through the three-dimensional spatial density function for pyrene-pyrene correlations. The $x-y$ plot shows a complex array of diffuse lobes, unlike smaller aromatics which show clear high density lobes between the C-H bonds.[11–14] The $x-z$ plot shows a very clear preference for molecules to be above/below the aromatic plane.

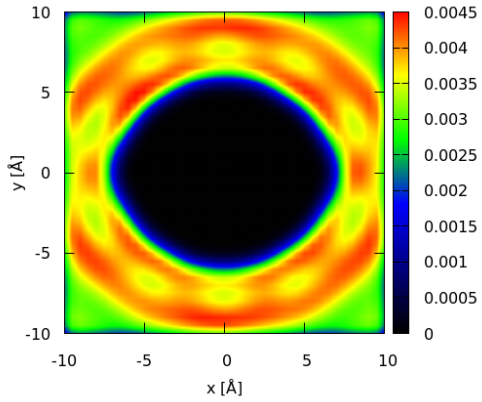

Figure S14: 2d slice through the pyrene-pyrene spatial density function in the xy plane (i.e. in the plane of the molecule).

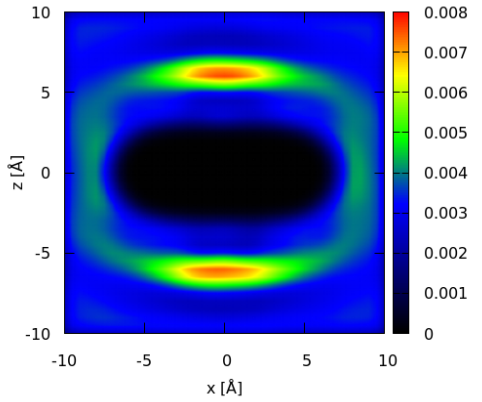

Figure S15: 2d slice through the pyrene-pyrene spatial density function in the xz plane where x is the long axis of the molcule and z is the axis normal to the aromatic plane.

In figure S16 the equivalent of the parallel stacked SDF as shown in figure 5 in the main text, but from an EPSR refined simulation where fixed OPLS charges are used in the reference potential.

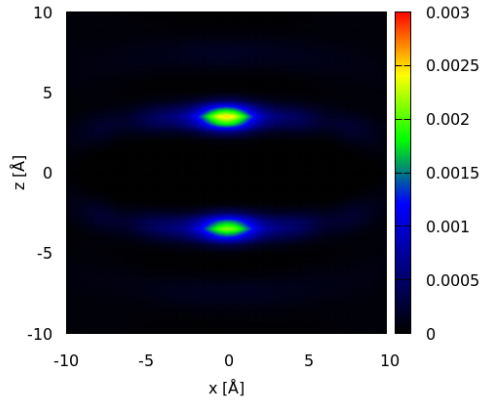

Figure S16: 2d slice through the pyrene-pyrene spatial density function for parallel molecules only in the xz plane, using OPLS fixed charges as the seed potential.

References

(1) Bowron, D. T.; Soper, A. K.; Jones, K.; Ansell, S.; Birch, S.; Norris, J.; Perrott, L.; Riedel, D.; Rhodes, N. J.; Wakefield, S. R.; Botti, A.; Ricci, M. A.; Grazzi, F.; Zoppi, M. NIMROD: The Near and InterMediate Range Order Diffractometer of the ISIS second target station. *Review of Scientific Instruments* **2010**, *81*.

(2) Soper, A. K. GudrunN and GudrunX: Programs for Correcting Raw Neutron and X-ray Diffraction Data to Differential Scattering Cross Section. 2011; `http://purl.org/net/epubs/work/56240`.

(3) Soper, A. K. Inelasticity corrections for time-of-flight and fixed wavelength neutron diffraction experiments. *Molecular Physics* **2009**, *107*, 1667–1684.

(4) Soper, A. K. The Radial Distribution Functions of Water as Derived from Radiation Total Scattering Experiments: Is There Anything We Can Say for Sure? *ISRN Physical Chemistry* **2013**, *2013*, 1–67.

(5) Soper, A. K. Partial structure factors from disordered materials diffraction data: An

approach using empirical potential structure refinement. *Physical Review B* **2005**, *72*, 104204.

(6) Soper, A. Empirical Potential Structure Refinement. `https://www.isis.stfc.ac.uk/Pages/Empirical-Potential-Structure-Refinement.aspx`.

(7) Westhaus, U.; Droge, T.; Sass, R. DETHERM®—a thermophysical property database. *Fluid Phase Equilibria* **1999**, *158-160*, 429–435.

(8) Gurevich, B.; Bednov, V. Study of temperature dependence of density and viscosity of aromatic substances. *Deposited Doc. VINITI* **1972**, 1–10.

(9) Hind, R. K.; McLaughlin, E.; Ubbelohde, A. R. Structure and thermal properties of liquids. Mutual molecular interference in the camphor + pyrene system. *Transactions of the Faraday Society* **1959**, *55*, 21–27.

(10) Dodda, L. S.; Vaca, I. C. D.; Tirado-Rives, J.; Jorgensen, W. L. LigParGen web server: an automatic OPLS-AA parameter generator for organic ligands. *Nucleic Acids Research* **2017**, *45*, W331–W336.

(11) Headen, T. F.; Cullen, P. L.; Patel, R.; Taylor, A.; Skipper, N. T. The structures of liquid pyridine and naphthalene: the effects of heteroatoms and core size on aromatic interactions. *Physical Chemistry Chemical Physics* **2018**, *20*, 2704–2715.

(12) Headen, T. F.; Howard, C. A.; Skipper, N. T.; Wilkinson, M. A.; Bowron, D. T.; Soper, A. K. Structure of pi-pi interactions in aromatic liquids. *Journal of the American Chemical Society* **2010**, *132*, 5735–42.

(13) Headen, T. F. Temperature dependent structural changes in liquid benzene studied using neutron diffraction. *Molecular Physics* **2019**, *117*, 3329–3336.

(14) F Headen, T.; Mino, C.; GA Youngs, T.; J Clancy, A. The structure of liquid thiophene

from total neutron scattering. *Physical Chemistry Chemical Physics* **2023**, *25*, 25157–25165.